Synthesis of a 1,2,3-bistriazole derivative of embelin and evaluation of its effect on high-fat diet fed-streptozotocin-induced type 2 diabetes in rats and molecular docking studies

Stalin, Antony

2020-03

Stalin , A , Kandhasamy , S , Kannan , B S , Verma , R S , Ignacimuthu , S , Kim , Y , Shao Qingsong , Chen , Y & Palani , P 2020 , ' Synthesis of a 1,2,3-bistriazole derivative of embelin and evaluation of its effect on high-fat diet fed-streptozotocin-induced type 2 diabetes in rats and molecular docking studies ' , Bioorganic Chemistry , vol. 96 , 103579 . https://doi.org/10.1016/j.b

http://hdl.handle.net/10138/339868
https://doi.org/10.1016/j.bioorg.2020.103579

Bioorganic Chemistry 96 (2020) 103579

Contents lists available at ScienceDirect

Bioorganic Chemistry

journal homepage: www.elsevier.com/locate/bioorg

Synthesis of a 1,2,3-bistriazole derivative of embelin and evaluation of its effect on high-fat diet fed-streptozotocin-induced type 2 diabetes in rats and molecular docking studies

Antony Stalin[a,b,c,*], Subramani Kandhasamy[d], Balakrishnan Senthamarai Kannan[e], Rama Shanker Verma[d], Savarimuthu Ignacimuthu[f], Yrjälä Kim[a,g], Shao Qingsong[a,b,*], Yuan Chen[a,b,*], Perumal Palani[c,*]

[a] State Key Laboratory of Subtropical Silviculture, Zhejiang A&F University, Hangzhou 311300, China
[b] Department of Traditional Chinese Medicine, Zhejiang A&F University, Hangzhou 311300, China
[c] Centre for Advanced Studies in Botany & Centre for Herbal Sciences, University of Madras, Guindy Campus, Chennai 600 025, Tamil Nadu, India
[d] Stem Cell and Molecular Biology Laboratory, Department of Biotechnology, Indian Institute of Technology Madras, Chennai 600036, Tamil Nadu, India
[e] Department of Chemistry, Tirunelveli Dakshinamara Nadar Sangam (TDMNS) College, Valliyur, Tirunelveli 627113, Tamil Nadu, India
[f] St. Xavier Research Foundation, St. Xavier's College, High Ground Road, Palayamkottai, Tirunelveli 627002,Tamil Nadu, India
[g] Department of Forest Sciences, PB 27 (Latokartanonkaari 7), 00014, University of Helsinki, Finland

ARTICLE INFO

InChIKey:
OIFDRKTZYPXNQF-UHFFFAOYSA-N*InChIKey:*
OIFDRKTZYPXNQF-UHFFFAOYSA-N*InChIKey:*
OIFDRKTZYPXNQF-UHFFFAOYSA-N*Keywords:*
Embelin-1,2,3-bistriazole
PPARγ partial agonist
Docking
Molecular stability

ABSTRACT

The embelin derivative **2a** was synthesized with the 1,2,3-bistriazole and spectral data confirmed its structural identity. Anti-diabetic and anti-lipidemic effects were evaluated using HFD-STZ induced type 2 diabetic rats. The derivative **2a** (30 mg/kg b wt.) supplementation significantly ($P \leq 0.01$) normalized the changed biochemical parameters like fasting blood glucose (FBG), body weights, plasma insulin level, total cholesterol (TC), triglycerides (TG) and marker enzymes of carbohydrate metabolism. The derivative **2a** (30 mg/kg) also showed a significant effect on oral glucose tolerance test (OGTT) and intraperitoneal insulin tolerance test (ITT). But 15 mg/kg dose of derivative **2a** failed to show any significant effects in HFD-STZ induced type2 diabetic rats. Histopathology analysis substantiated the protective effect of this derivative **2a** (30 mg/kg b wt.) on the β-cells of the pancreatic, liver and adipose tissues in diabetic treated rats. Further, the expressions of PPARγ and GLUT4 were significantly enhanced in the epididymal adipose tissue. The HOMO and LUMO energies characterized the molecular stability of the derivative **2a** with 6-311G++ (d, p) in DFT/B3LYP/LanL2DZ method using Gaussian09 program package. The molecular docking analysis also confirmed the activity of derivative **2a** through hydrogen bond interaction with ARG 288, GLU 343, SER 342 and least energy value (−7.72 kcal/mol). Hence, the embelin-1,2,3-bis triazole derivative **2a** (30 mg/kg) enhanced the activity of embelin and might be acting as a suitable drug for type 2 diabetes, obesity and its complications.

1. Introduction

Type 2 diabetes mellitus (T2DM) is an endocrine-metabolic disease characterized by insulin resistance and insulin secretion defects that can be demonstrated through several alterations in carbohydrates, lipids, and protein metabolism. It caused by metabolic dysregulations like decreased utilization of glucose linked with slanted insulin signaling cascade. Also, insulin resistance decreases the insulin secretion and β-cell mass in the peripheral tissues that lead to β-cell dysfunction [1,2].

PPARs, the nuclear receptor superfamily plays a specific role in glucose and energy metabolism. It acts as the primary target for ligand inducible transcription factors that regulates glucose and lipid metabolism [1–3]. PPARγ has different tissue distributions in the adipose, skeletal muscle, and hepatic tissues based on insulin sensitivity and its reactions to the drugs are significantly different [3–5]. Specifically,

* Corresponding authors at: State Key Laboratory of Subtropical Silviculture, Zhejiang A&F University, Hangzhou 311300, China (A. Stalin). Department of Traditional Chinese Medicine, Zhejiang A&F University, Hangzhou 311300, China (A. Stalin, Q. Shao and Y. Chen). Centre for Advanced Studies in Botany & Centre for Herbal Sciences, University of Madras, Guindy Campus, Chennai 600 025, India (A. Stalin and P. Palani).
E-mail addresses: a.staanlin@gmail.com, stalinantony@zafu.edu.cn (A. Stalin), sqszjfc@126.com (Q. Shao), ychen@zafu.edu.cn (Y. Chen), palani7@unom.ac.in (P. Palani).

https://doi.org/10.1016/j.bioorg.2020.103579
Received 24 September 2019; Received in revised form 19 December 2019; Accepted 10 January 2020
Available online 10 January 2020

activation of PPARγ improved the insulin sensitivity in adipose tissue through adipokines production leads to glucose homeostasis, lipogenesis and adipogenesis [6–8]. Thiazolidinediones (TZDs) group of drugs such as rosiglitazone and pioglitazone are the well-known PPARγ activators. Due to the various adverse effects such as osteoporosis, hepatotoxicity, water and sodium retention and inducing the risk of cancer, they have been withdrawn from the market [9]. Hence, there is a demand to develop better PPARγ activators for eradicating insulin resistance conditions [10].

The natural product extracts possess secondary metabolites and integrative bioactive ingredients that serve as valuable medicinal sources in emerging new drugs for hysterical diseases. Embelin is a benzoquinone component of *Embelia ribes* Burm. from the *Myrsinaceae* family [11–15]. The alkyl substitution of 1,4-benzoquinone core possesses many biological properties such as anti-diabetic, anti-inflammatory, antihelminthic, antimicrobial, analgesic, antioxidant, anticancer, wound healing, and cardio-protective activities [16]. Many quinones containing triazoles have been documented from natural sources, especially in traditional medicinal plants. In recent years, the triazole substituted quinones have strong biochemical and pharmacological properties that attract many clinical applications.

1,2,3-bistriazole heterocyclic compounds continue to be an exploding field in pharmaceutical chemistry [17,18]. Modern trends in organic chemistry are driving more towards the novel synthesis of highly potential biomolecules, which are useful as drugs in clinical research [19–21]. The potency of triazole is measured in terms of toxicity, dosage and effective binding to specific receptor sites to control the replication of harmful microorganisms thereby inhibition of neglected disease [22]. 1,2,3-bistriazoles are one of the important components in the field of medicinal and organic chemistry because of the presence of nitrogen heterocycles [23–25]. It has various, exciting pharmacological properties such as antitubercular [26], anti-HIV [27], antimalarial [28], antiepileptic [29], antiallergic [30], antileishmanial [31–33], antifungal [34,35] and anticancer activities [36]. Due to the astounding features of oxygen and nitrogen-based biomolecules, it has been utilized in inhibition of intracellular proinflammatory mediators, reduction of lipid levels and in managing severe hyperglycemia and enhancement of oxidative stress in the diabetic treatment [37,38]. Embelin and some of its derivatives have been proven for their antidiabetic activity through the utilization of glucose in peripheral tissues [11,39].

In the field of organic synthesis and theoretical chemistry, 1,2,3-bistriazoles have played a significant role in the development of biologically active compounds [40–42]. Based on the above facts, the present study was designed to synthesize 1,2,3-bistriazole derivative of embelin and evaluate its effects on high-fat diet (HFD) fed-streptozotocin (STZ) - induced type 2 diabetes in rats, using microscopic, physiological and biochemical studies.

2. Results and discussion

Benzoquinone types of molecules derived from medicinal plants have been shown to entail progressive effects in the management of obesity, diabetes and associated ailments [11–14]. A large number of benzoquinone derivatives have been synthesized and reported for their various activities, including anti-diabetic activity [43]. Already, we investigated and reported the anti-diabetic activity of two embelin derivatives (6–bromoembelin (2) and vilangin (3)) [39].

In the current study, the novel embelin-based 1,2,3-bistriazole (**2a**) (alkyl substitution of 1,4-benzoquinone by (1,2,3)-triazoles moieties) derivative was synthesized to accelerate the antidiabetic activity in HFD fed-STZ-induced type2 diabetic rats. The combination of HFD and a low dose of STZ induce hyperinsulinemia in the mode of impaired glucose tolerance with dyslipidemia, hyperglycemia, and destruction in the function of β-cell witnessed in the Wistar rats. Due to the resemblance of these metabolic characteristics to the human T2DM, this kind of animal models has preferable been used to generate the obesity-linked T2DM [44–49].

2.1. Chemistry

The embelin-based 1,2,3-bistriazole derivative (**2a**) was synthesized by propargylation followed by click chemistry reaction in scheme 1. Synthesized embelin bis-triazole derivative was illustrated by ^{1}H & ^{13}C NMR, IR and MS (mass spectra) analysis for structural confirmation. In the spectral confirmation of compound **2a**, FT-IR spectrum functional group confirmation exhibited a broad band at 1709 cm^{-1} corresponding to a carbonyl group (C═O), aromatic carbon–carbon stretching (C—C) was present at 1642 cm^{-1}, and triazole containing carbon-nitrogen (C—N) was shown at 2322 cm^{-1}, respectively. The proton NMR spectrum of molecule **2a** shows the exact peaks in the range 6.99–7.87 ppm, integrating fourteen protons corresponding to aromatic protons. The embelin core containing one aromatic proton is depicted as a singlet at 5.60 ppm; the peak at 5.51 ppm integrating four protons confirms the presence of triazole attached benzyl $-CH_2$ protons and peaks ranging from 0.86 to 2.09 ppm represent twenty-three aliphatic protons integrated for confirmation of protons containing embelin side chain. ^{13}C NMR spectrum in $CDCl_3$ depicts two quinone carbonyl carbons (—C═O) at 172.63 ppm and 200.03 ppm and the peaks ranging from 124.04 ppm to 152.16 ppm show the presence of aromatic carbons. The peak at 98.67 ppm confirms an iodine attached carbon (—C—I) in the aromatic ring, the peak at 83.05 ppm corresponds to embelin containing aromatic —CH carbon and aliphatic side chain containing carbons are present at 14.27–30.00 ppm depicted for compound **2a**. ESI-MS for compound **2a** showed a peak at *m/z* 889.19 for $[M + H]^+$ ion, which confirms the formation of the product (See supplementary information: Figs. 1–3).

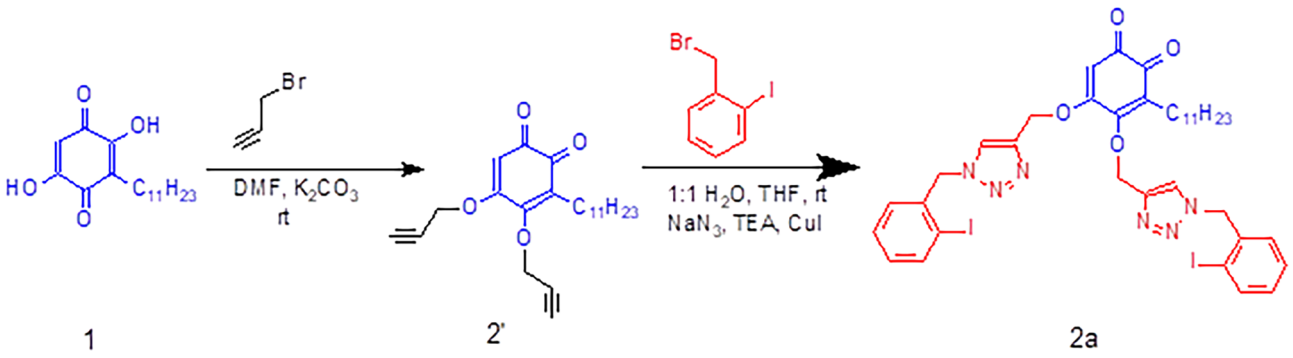

Scheme 1. Schematic representation for the synthesis of embelin-based 1,2,3-bistriazole diversified system.

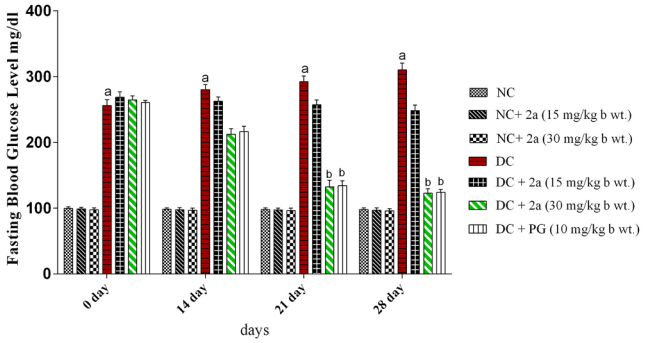

Fig. 1. Alteration of derivative **2a** on FBG in experimental rats. DC – Diabetic Control, NC – Normal Control, 2a – derivative **2a** (15 mg/kg and 30 mg/kg b wt.), PG – Pioglitazone. Values indicate mean ± standard error of the mean (SEM) of six rats per group. [a]Significantly different from the normal control group ($P \leq 0.01$); [b]Significantly different from the diabetic control group ($P \leq 0.01$).

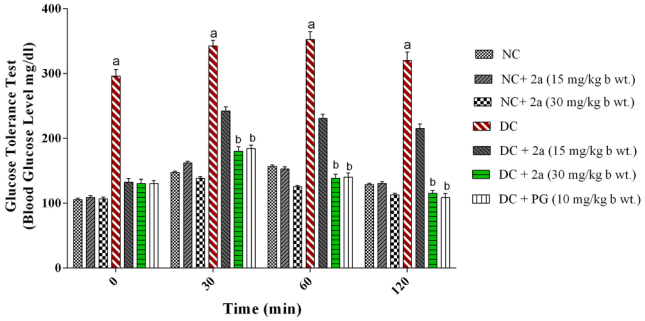

Fig. 2. Alteration of derivative **2a** on oral glucose tolerance levels of experimental rats by OGTT. DC – Diabetic Control, NC – Normal Control, **2a** – derivative **2a** (15 mg/kg and 30 mg/kg b wt.), PG – Pioglitazone. Values indicate mean ± standard error of the mean (SEM) of six rats per group, [a]Significantly different from the normal control group ($P \leq 0.01$); [b]Significantly different from the diabetic control group ($P \leq 0.01$).

2.2. Biological evaluation

2.2.1. Effect of derivative on FBG

The results of FBG analysis showed that treatment with a higher dose of **2a** (30 mg/kg) and pioglitazone (10 mg/kg) significantly reduced the blood glucose levels in a HFD fed-STZ-induced type 2 diabetic rats. The reductions of blood glucose levels in **2a** (30 mg/kg) treated animals were found to be 67.98% ($P \leq 0.01$) and 81.11% ($P \leq 0.01$) on day 21 and day 28, respectively. Whereas, pioglitazone reduced the blood glucose level by 68.53% ($P \leq 0.01$) and 82.04% ($P \leq 0.01$), respectively. Treatment with a lower dose of **2a** (15 mg/kg) to HFD fed-STZ-induced type 2 diabetic rats also lowered the blood glucose levels on day 21 (13.59%) and day 28 (25.04%) but results are statistically insignificant (Fig. 1).

2.2.2. Effect of derivative on plasma insulin

The diabetic rats treated by the derivative **2a** (30 mg/kg) and pioglitazone significantly ($P \leq 0.01$) decreased the levels of elevated plasma insulin (79.15%, and 76.59% respectively) to near normal on day 28. But 15 mg/kg dose of derivative **2a** failed to show a significant reduction in plasma insulin level (31.44%) (Table 1). The administration of derivative **2a** (30 mg/kg) on diabetic rats prompted a significant reduction in FBG and plasma insulin levels, thereby decreasing the insulin resistance condition and improving the insulin sensitivity and β-cell function in peripheral tissues [50,51].

2.2.3. Effect of derivative on OGTT

In OGTT, glucose was orally administered to the rats and the levels were assessed. After 30 min, the plasma glucose levels were increased in the normal and diabetic rats (Fig. 2). The rats treated by derivative **2a** (30 mg/kg) significantly ($P \leq 0.01$) reduced the glucose level at 60 and 120 min (30.12% and 36.22%, respectively). Similarly, pioglitazone treated rats also reduced the elevated glucose level (31.48% and 41.06%, respectively). But, the plasma glucose levels were not significantly reduced in the diabetic rats treated by 15 mg/kg dose of the derivative **2a** at 60 and 120 min (5.08% and 12.51%, respectively).

2.2.4. Effect of derivative on ITT

ITT also exhibited a significant ($P \leq 0.01$) glucose reduction in diabetic rats administered with the derivative **2a** (30 mg/kg) and pioglitazone at 30 min (68.14%, 67.52% respectively) and 60 min (71.37%, 70.24%, respectively). But, the 15 mg/kg dose of derivative **2a** did not show a significant glucose reduction on 30 and 60 min (12.60% and 18.33%, respectively) (Table 1). These results confirmed that the derivative **2a** (30 mg/kg) regulated the insulin-dependent glucose clearance into the peripheral tissues and revealed their influence in elevating the short-time glucose homeostasis. [52,53]

2.2.5. Effect of derivative on body weight, and lipid profiles

During the experiment, a significant body weight gain with increased levels of serum TC, TG, and FFA was noticed in the diabetic control rats. This is due to the intracellular lipid accumulation in the adipose cells by increasing the size of epididymal adipose cells resulting in a significant increase in body weight [46,54,55]. After 28 days of experiment, the derivative **2a** (30 mg/kg) and pioglitazone administered diabetic rats had significantly ($P \leq 0.01$) lowered the levels of TC (30.44% and 15.53%, respectively), TG (65.55% and 16.92%, respectively) and FFA (54.34% and 27.19%, respectively) (Table 2). However, the levels of TC (7.76%), TG (10.67%) and FFA (10.14%) for the derivative **2a** (15 mg/kg) treated rats are statistically insignificant.

The derivative **2a** (30 mg/kg) was sufficient to control the increased lipid accumulation and significantly ($P \leq 0.01$) reduced the size of adipose tissue and reversed the increased body weight on 21st (15.90%)

Table 1
Impact of derivative **2a** on Plasma insulin and glucose level (ITT) in experimental rats.

Groups	Plasma insulin (μU/ml) 0 day	28th day	Blood glucose level (mg/dl) 0 min	30 min	60 min
Normal control	16.26 ± 0.46	16.78 ± 0.44	130.24 ± 3.4	106.34 ± 2.6	98.2 ± 1.4
Normal + **2a** (15 mg/kg b wt.)	16.34 ± 0.62	15.38 ± 0.36	122.34 ± 2.8	106.26 ± 3.6	98.84 ± 2.4
Normal + **2a** (30 mg/kg b wt.)	15.48 ± 0.74	15.64 ± 0.22	120.26 ± 2.6	100.24 ± 3.4	96.20 ± 2.2
Diabetic control	26.34 ± 0.80[a]	29.81 ± 0.84[a]	324.20 ± 8.4[a]	320.80 ± 4.2[a]	316.50 ± 4.2[a]
Diabetic + **2a** (15 mg/kg b wt.)	25.86 ± 0.32	22.68 ± 0.42	138.60 ± 3.6	280.40 ± 3.2	258.48 ± 5.8
Diabetic + **2a** (30 mg/kg b wt.)	23.39 ± 0.44	14.64 ± 1.22[b]	134.80 ± 4.2[b]	102.22 ± 4.2[b]	90.62 ± 6.2[b]
Diabetic + Pioglitazone (10 mg/kg b wt.)	24.26 ± 0.24	16.88 ± 0.63[b]	136.2 ± 3.6[b]	104.20 ± 5.4[b]	94.20 ± 5.4[b]

Values indicate mean ± standard error of the mean (SEM) of six rats per group.
[a] $P \leq 0.01$, compared with normal control values.
[b] $P \leq 0.01$, compared with diabetic control values.

Table 2
Impact of derivative **2a** on TC, TG and FFA levels in experimental rats.

Groups	TC (mg/dl)	TG (mg/dl)	FFA (mg/dl)
Normal control	74.62 ± 2.42	76.42 ± 1.54	44.44 ± 1.24
Normal + **2a** (15 mg/kg b wt.)	76.46 ± 1.12	76.28 ± 1.14	44.68 ± 1.36
Normal + **2a** (30 mg/kg b wt.)	76.26 ± 2.34	75.74 ± 5.44	42.84 ± 1.28
Diabetic control	98.64 ± 4.86[a]	146.48 ± 4.82[a]	108.44 ± 5.24[a]
Diabetic + **2a** (15 mg/kg b wt.)	91.54 ± 3.42	132.36 ± 2.84	98.46 ± 4.84
Diabetic + **2a** (30 mg/kg b wt.)	75.62 ± 2.24[b]	88.48 ± 1.46[b]	70.26 ± 4.24[b]
Diabetic + Pioglitazone (10 mg/kg b wt.)	85.38 ± 2.36	125.28 ± 2.46	85.26 ± 5.24[b]

Values indicate mean ± standard error of the mean (SEM) of six rats per group.
[a] Significantly different from the normal control group ($P \leq 0.01$);
[b] Significantly different from the diabetic control group ($P \leq 0.01$).

Table 3
Impact of derivative **2a** on body weight in experimental rats.

Groups	Body weight (g) 0 day	14th day	21st day	28th day
Normal control	188.28 ± 10.24	190.42 ± 10.28	196.34 ± 12.26	198.46 ± 12.42
Normal + **2a** (15 mg/kg b wt.)	186.44 ± 7.68	192.86 ± 10.42	195.48 ± 8.64	199.84 ± 10.48
Normal + **2a** (30 mg/kg b wt.)	185.64 ± 2.24	192.52 ± 11.24	194.42 ± 10.48	199.24 ± 6.28
Diabetic control	184.12 ± 12.10	200.24 ± 12.22	234.54 ± 12.48[a]	260.48 ± 10.68[a]
Diabetic + **2a** (15 mg/kg b wt.)	186.28 ± 10.84	198.34 ± 12.26	230.56 ± 12.84	242.56 ± 10.56
Diabetic + **2a** (30 mg/kg b wt.)	184.44 ± 11.26	194.26 ± 10.62	202.38 ± 12.26	204.42 ± 10.26[b]
Diabetic + Pioglitazone (10 mg/kg b wt.)	186.44 ± 12.26	196.34 ± 9.24	229.38 ± 11.84	238.28 ± 10.42

Values indicate mean ± standard error of the mean (SEM) of six rats per group.
[a] Significantly different from the normal control group ($P \leq 0.01$).
[b] Significantly different from the diabetic control group ($P \leq 0.01$).

and 28th (27.42%) days, respectively [39,56]. The diabetic rats treated by 15 mg/kg dose of derivative **2a** and pioglitazone, however, did not show a significant weight reduction on 21st (1.73%, 2.25%, respectively) and 28th day (7.39%, 9.32%, respectively) (Table 3).

2.2.6. Effect on liver enzymes

In the liver, STZ creates toxicity and modifies its shape and functions [57–59] and leads to decreased activities of essential liver enzymes such as hexokinase, glucose-6-phosphatase and fructose-1, 6-bisphosphatase enzymes. The derivative **2a** (30 mg/kg) and pioglitazone administered diabetic rats had significantly ($P \leq 0.01$) improved the activities near to standard levels for hexokinase (67.39% and 60.87%, respectively), glucose-6-phosphatase (47.50% and 45.00%, respectively) and fructose-1 6-bisphosphatase (24.40% and 26.83%, respectively) enzymes. But, the diabetic rats treated with 15 mg/kg dose of derivative **2a** showed no significant effect (2.54%, 5.00% and 4.88% respectively) (Table 4).

2.2.7. Gene, protein expressions of PPARγ and GLUT4

Due to the insulin resistance, the lipid and glucose metabolism affects T2DM that leads to the down regulation of PPARγ in adipose, skeletal muscle, and hepatic tissues. By the activation of PPARγ, the tissues have been up-regulated to reverse the insulin resistance condition [60–64]. In our study, the PPARγ gene and protein expression significantly ($P \leq 0.01$) increased in the epididymal adipose tissue through the treatment of derivative **2a** (30 mg/kg) in HFD-STZ induced diabetic rats (Figs. 3 and 4). The expression of PPARγ was, however, slightly increased in the skeletal muscle and liver (data not shown).

In the glucose transporter family, glucose transporter 4 (GLUT4) is one of the main subtypes present in adipose tissues, skeletal muscle, and heart [65,66]. By the activation of GLUT4, translocation and activation regulate the glucose homeostasis that leads to glucose clearance into peripheral tissues [67,68].

According to Suzuki et al., the translocation and activation of GLUT4 could not properly occur under the insulin resistance condition causing the elevation of glucose level in T2DM [65,66]. Hence, the GLUT4 mRNA and protein expression levels down regulated in the skeletal muscles and adipose tissue [46,66,69]. We also found a decreased expression of GLUT4 mRNA and protein in the epididymal adipose tissue of diabetic rats. The treatment by derivative **2a** (30 mg/kg) significantly ($P \leq 0.01$) improved the expression of GLUT4 mRNA and protein levels recorded in the epididymal adipose tissue of treated

Table 4
Impact of derivative **2a** on hexokinase, glucose-6-phosphatase, and fructose-1,6-bisphosphatase and in experimental rats.

Groups	Hexokinase (U/mg protein/min)	Glucose-6- phosphatase (U/mg protein/min)	Fructose-1,6- bisphosphatase (U/mg protein/min)
Normal control	7.80 ± 0.4	0.40 ± 0.1	0.42 ± 0.2
Normal + **2a** (15 mg/kg b wt.)	7.62 ± 0.2	0.39 ± 0.1	0.41 ± 0.1
Normal + **2a** (30 mg/kg b wt.)	7.26 ± 0.6	0.36 ± 0.2	0.35 ± 0.4
Diabetic control	4.60 ± 0.2[a]	0.80 ± 0.2[a]	0.82 ± 0.2[a]
Diabetic + **2a** (15 mg/kg b wt.)	4.72 ± 0.2	0.76 ± 0.1	0.78 ± 0.2
Diabetic + **2a** (30 mg/kg b wt.)	7.70 ± 0.5[b]	0.42 ± 0.1[b]	0.62 ± 0.3[b]
Diabetic + Pioglitazone (10 mg/kg b wt.)	7.40 ± 0.6[b]	0.44 ± 0.2[b]	0.60 ± 0.4[b]

Values indicate mean ± standard error of the mean (SEM) of six rats per group.
[a] $P \leq 0.01$, compared with normal control values.
[b] $P \leq 0.01$, compared with diabetic control values.

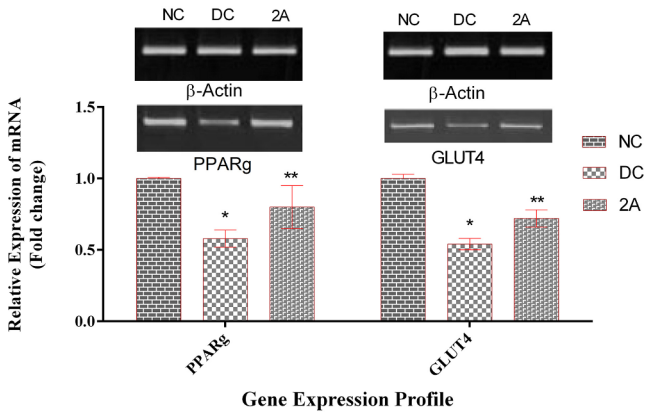

Fig. 3. mRNA expression of derivative **2a** on PPARγ and GLUT4 in adipose tissue. NC – Normal Control (30 mg/kg b wt.), DC – Diabetic Control (30 mg/kg b wt.), **2a** – derivative **2a** (30 mg/kg b wt.) Bars are represented as means ± SEM for three independent experiments performed. *Significantly different from the normal control group ($P \leq 0.01$); **significantly different from the diabetic control group ($P \leq 0.01$).

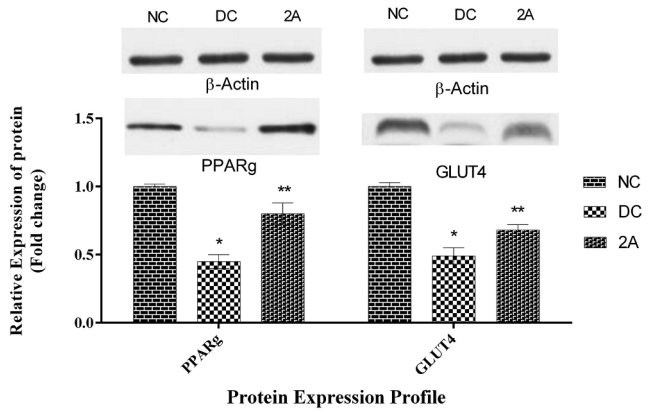

Fig. 4. Protein expression of derivative **2a** on PPARγ and GLUT4 in adipose tissue. NC – Normal Control, DC – Diabetic Control, **2a** – derivative **2a** (30 mg/kg b wt.). Bars are represented as means ± SEM for three independent experiments performed. *Significantly different from the normal control group ($P \leq 0.01$); **significantly different from the diabetic control group ($P \leq 0.01$).

diabetic rats (Figs. 3 and 4). These findings are in agreement with earlier reports [70,71,72]. Since the derivative **2a** (15 mg/kg) didn't show a significant effect in blood glucose levels and other biochemical parameters, the gene and protein expression levels were not studied.

2.2.8. *Histopathology analysis*

The pancreatic islet cells, liver and intra-peritoneal adipose tissues of experimental rats were subjected to the histo-pathological analysis. The β-cells of the pancreas with granulated cytoplasm and uniform nuclei were detected in the tissues of the normal control rats (Fig. 5A). In T2DM, pancreatic β-cells have been affected by the peripheral insulin resistance, which is correlated with inadequate insulin secretion [73–76]. As reported earlier, in the current study, we found de-granulated and functionally decreased pancreatic β-cells and lesions [77,78] in the untreated diabetic control rats (Fig. 5B). Histology in the tissues of treated diabetic groups by the derivative **2a** (30 mg/kg) and pioglitazone showed re-granulation in tissues and β-cells development (Fig. 5C, D).

The histology of HFD diabetic control rats showed fatty changes in the liver (Fig. 6B) and there are no changes observed in normal rats (Fig. 6A), while the treatment with derivative **2a** (30 mg/kg) and pioglitazone lowered the amount of fat accumulation in the treated rats

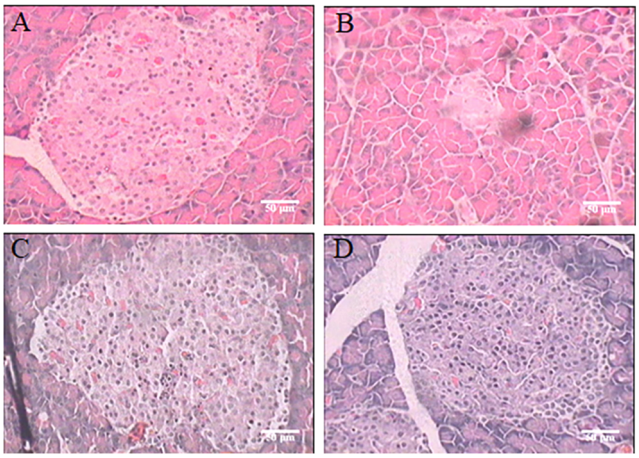

Fig. 5. Histological alterations in the derivative **2a** treated islets of pancreas in experimental rats (H & E, 40×) A - Normal control, B - Diabetic control, C - Diabetic + **2a** (30 mg/kg b wt.), D - Diabetic + Pioglitazone (10 mg/kg b wt.)

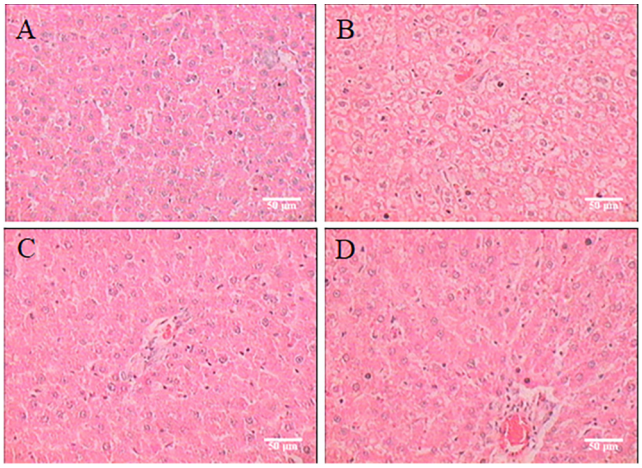

Fig. 6. Histological alterations in the derivative **2a** treated islets of Liver in experimental rats (H & E, 40×) A - Normal control, B - Diabetic control, C - Diabetic + **2a** (30 mg/kg b wt.), D - Diabetic + Pioglitazone (10 mg/kg b wt.)

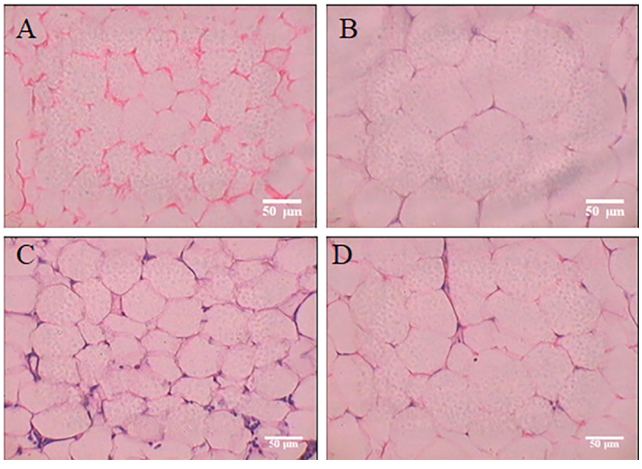

Fig. 7. Histological alterations in the derivative **2a** treated islets of Adipose Tissue in experimental rats (H & E, 40 ×) A - Normal control, B - Diabetic control, C - Diabetic + **2a** (30 mg/kg b wt.), D - Diabetic + Pioglitazone (10 mg/kg b wt.)

(Fig. 6C, D). The histological data support that the derivative **2a** (30 mg/kg) improved the liver cellular count and helped to decrease the blood glucose level [58,79]. Similarly, in the HFD diabetic control rats showed the hypertrophy in the histology of the intra-peritoneal adipose tissue (Fig. 7B) and no changes were observed in normal rats (Fig. 7A); in the treated rats the amount of hypertrophy was reduced (Fig. 7C, D). Hence, the derivative **2a** (30 mg/kg) significantly enhanced the function and arrangement of hepatic cells thereby decreasing the complications of diabetes mellitus [58,79]. The results are in correlation with the biochemical parameters, as mentioned before. Since the derivative 2a (15 mg/kg) didn't show a significant effect in blood glucose levels and other biochemical parameters, the histo-pathological analysis was omitted.

2.3. Theoretical analysis

2.3.1. HOMO-LUMO analysis

The frontier orbitals and parameters of the molecules play a vital role in drug design and in recognizing their reactivity. The HOMO and LUMO energies characterize the capability of electron-donating and withdrawing ability, respectively, and the energy gap (ΔE) between HOMO and LUMO illustrates the stability of the molecular surface [80]. The red and green colors stand for the positive and negative phases of the molecule, respectively. The higher E_{HOMO} value indicates larger feasibility of the molecule to donate electrons and smaller E_{LUMO} value of the molecules has more feasibility to accept electrons. The small value of ΔE relates to lower kinetic stability and better chemical reactivity [81–83]. The electronic transition absorption corresponds to the transition from HOMO to the LUMO through electron transfer (Fig. 8) [84].

As can be seen from the figure (Fig. 9), the electron density of HOMO (−3.326 eV) and HOMO-1 (−6.079 eV) of **2a** are located and predominantly stretched over uncharged triazole to quinone rings. The HOMO-1(−6.079 eV) is significantly positioned on the quinone ring alone. The LUMO (−2.909 eV) is situated largely over the quinone ring with partially spread over the triazole ring. The LUMO + 1 (−2.452 eV) specifically resides over triazole and benzene rings. The computed HOMO-LUMO energy gap was found to be 0.417 eV, shown in figure (Fig. 8).

For 6-bromoembelin **(2)** (Fig. 10), the HOMO (−7.072 eV) resided on the quinone ring, mainly on one oxygen and bromine atoms and extended over few bonds of the uncharged alkyl chain, whereas LUMO (−3.781 eV) occupied the quinone ring particularly on two oxygen atoms and not on bromine atom. This is illustrated in figure (Fig. 8); the calculated HOMO-LUMO energy gap was 3.291 eV.

For embelin (1) (Fig. 11), the HOMO (−6.999 eV) was largely crowded over on the quinone ring, mainly on one oxygen atom and extended over few bonds of uncharged alkyl chain, whereas LUMO (−3.563 eV) occupied the quinone ring mainly two oxygen atoms (Fig. 8). The computed HOMO-LUMO energy gap was 3.436 eV.

2.3.2. Theoretical analysis of chemical reactivity

The frontier orbital energies exhibit various properties like the chemical potential (μ), chemical hardness (η), and electrophilicity index (ω) given in Table 5. According to Koopmans's theorem and Parr approximation, the μ, η, and ω can be calculated using HOMO and LUMO energies using the relation [85,86]:

$$\mu = (E_{HOMO} + E_{LUMO})/2 \quad (1)$$

$$\eta = (E_{LUMO} - E_{HOMO})/2 \quad (2)$$

$$\omega = \mu^2/2\eta \quad (3)$$

$$\text{Chemical softness } S = 1/(E_{LUMO} - E_{HOMO}) \quad (4)$$

The electrophilicity index (ω) discloses the stabilization energy of the molecule received as an electronic charge from the adjacent environment. The results indicated that the derivative **2a** containing quinoline conjugated triazole molecule is more reactive. The introduction of triazole groups at the para-position of the aromatic ring in **2a**, yielded greater effect of electrophilic compounds at their singlet ground state state (i.e., ω = 23.306 eV for **2a** > ωN = 8.948 eV for 2 > ωN = 8.117 eV for 1) than 6-Bromoembelin (2) and Embelin (1).

The hardness η indicates the reactivity of the molecule, and the hardness of the molecules increased in the following order **2a** < **2** < **1,** indicating that **2a** had relatively higher reactivity and more easily polarisable than 2 and 1. A rigid molecule with a substantial HOMO-LUMO gap with elevated excitation energies was essential to a manifold of excited states, was less reactive and the electron density was harder to change than for a soft molecule.

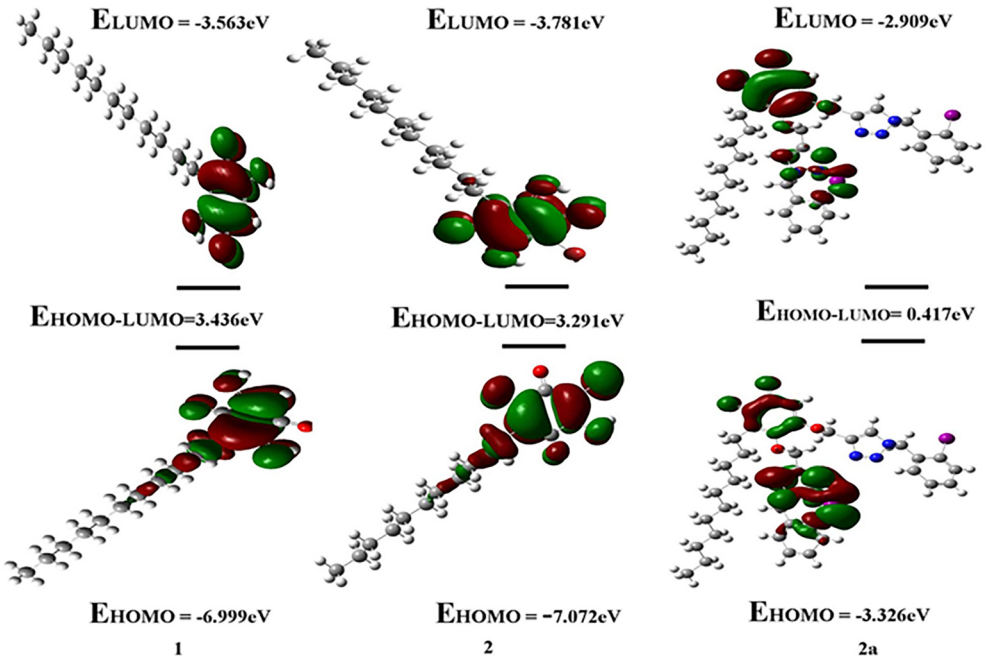

Fig. 8. Electron density distribution and the energies (eV) of HOMOs and LUMOs for three compounds 1, 2 and **2a.**

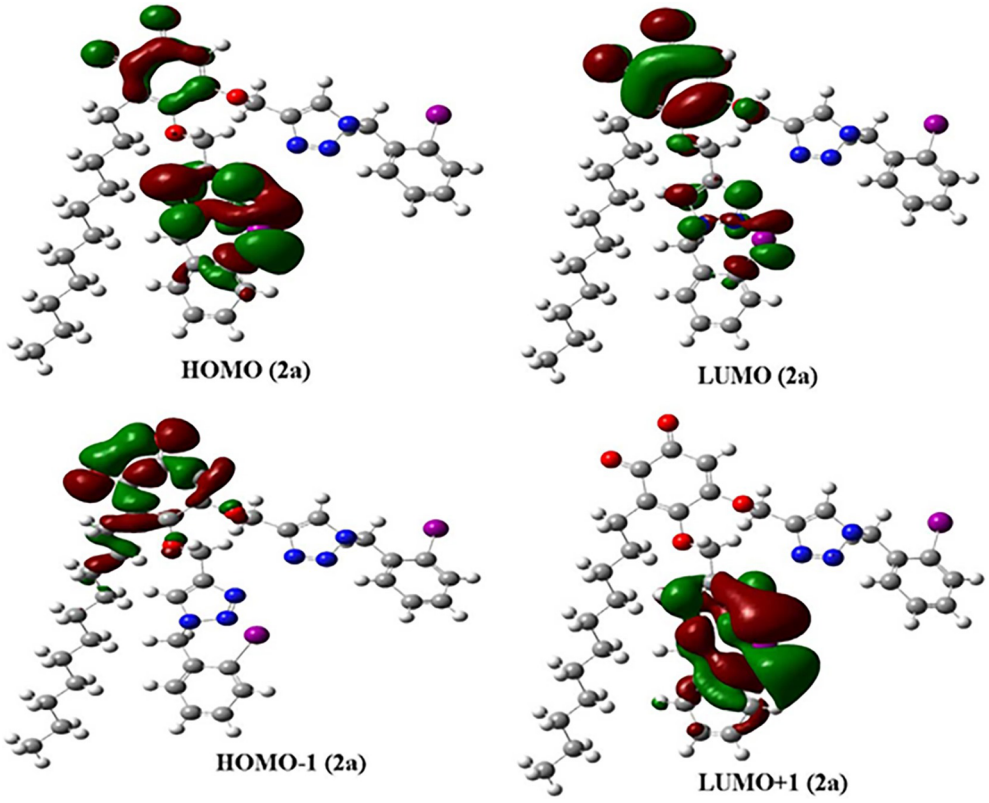

Fig. 9. Frontier molecular orbitals for the electronic transitions of derivative **2a** as reported at B3LYP/LanL2DZ level using GAUSSIAN09 package.

2.3.3. Electrostatic potential analysis

The investigation of Molecular electrostatic potential (ESP) receives much attention due to the electrostatic property of molecules. The electrostatic potential of the molecule can easily be correlated to its performance, such as electrophilic and nucleophilic reactions for the study of biological recognition processes [87], and hydrogen bonding interactions. Besides, it can be used to infer the variety of physical and chemical features including non-covalent interactions in complex

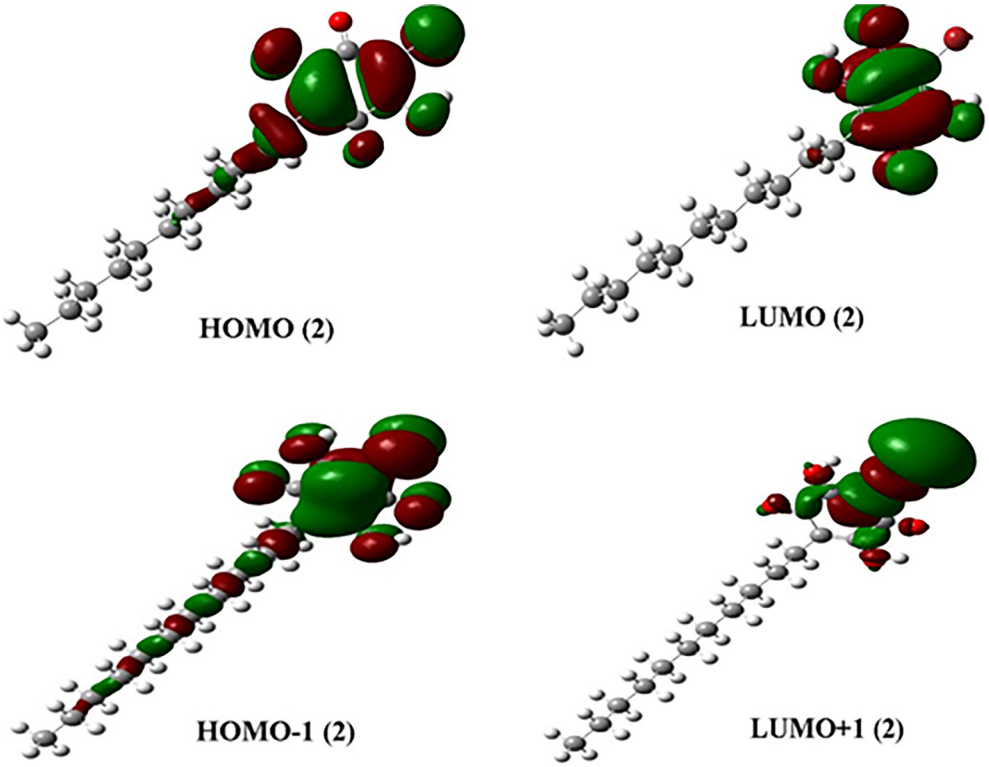

Fig. 10. Frontier molecular orbitals for the electronic transitions of derivative **2** as reported at B3LYP/6311G++(d,p) level using GAUSSIAN09 package.

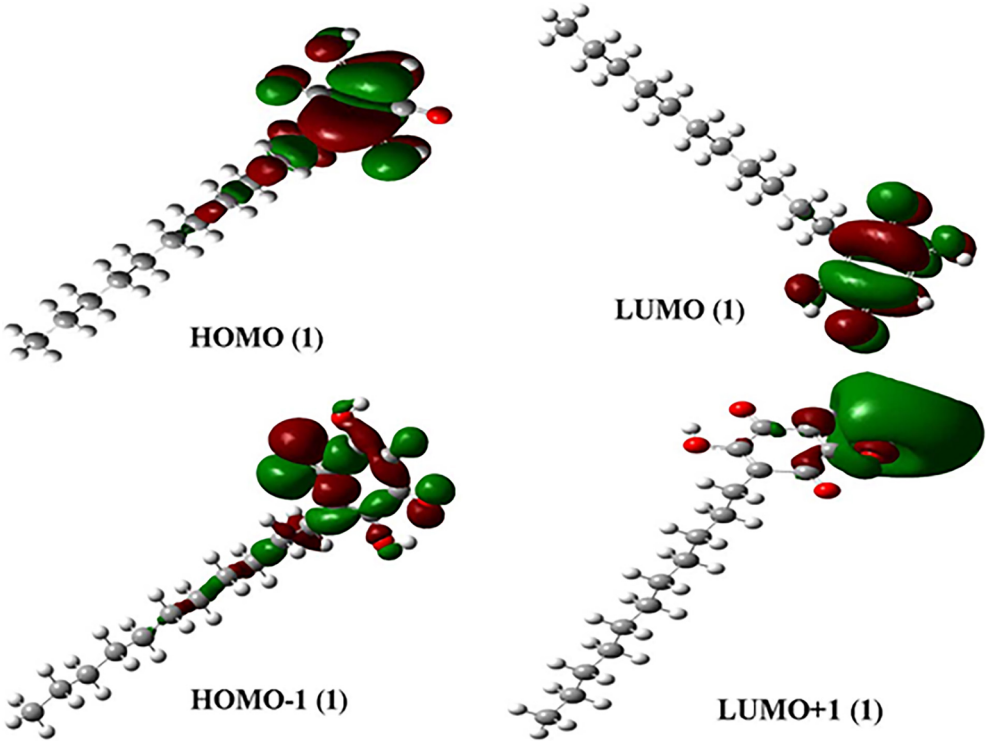

Fig. 11. Frontier molecular orbitals for the electronic transitions of compound **1** as reported at B3LYP/6311G++(d,p) level using GAUSSIAN09 package.

Table 5
Calculated energy values of derivatives **2a**, **6-Bromoembelin (2) and Embelin (1)**.

Compounds	E_{HOMO} (eV)	E_{LUMO} (eV)	$\Delta E = E_{LUMO} - E_{HOMO}$ (eV)	Chemical Potential μ (eV)	Chemical Hardness η (eV)	Electrophilicity ω (eV)	Chemical Softness S (eV)
2a	−3.326	−2.909	0.417	−3.118	0.2085	23.306	2.398
6-Bromoembelin (2)	−7.072	−3.781	3.291	−5.427	1.6455	8.948	0.304
Embelin (1)	−6.999	−3.563	3.436	−5.281	1.718	8.117	0.291

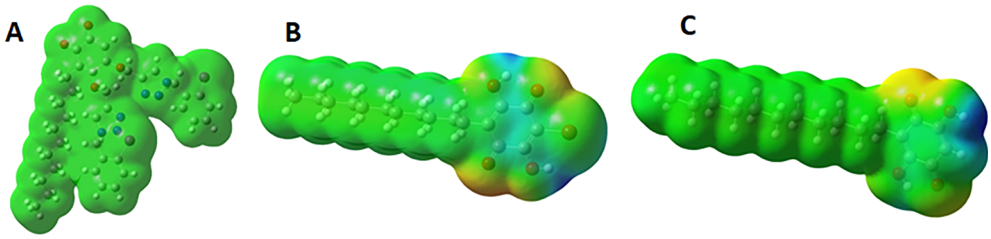

Fig. 12. 3D molecular electrostatic potential surface of derivatives **2a** (A), **2** (B), and **1** (C).

biological systems [88]. The negative ESP surface can act as nucleophilic sites (electron-rich centres) indicated as red shades.

Similarly, a positive ESP surface can act as electrophilic sites (electron-deficient centres) shown as blue shades. Green shades indicate neutral sites. The molecular electrostatic potential was calculated to determine the active sites for nucleophilic and electrophilic attack for the compounds **2a**, 2 and 1 in optimized geometry. A potential increase on the molecular surface is shown in the order blue < green < red. The electrostatic potential diagrams of systems such as **2a**, 2 and 1 are shown in figure (Fig. 12). The electrostatic potential diagram of **2a** (Fig. 12A) showed that the entire molecule is neutral. The ESP diagram (Fig. 12B) of system 2 showed several sites of negative character including O20, and O21 atoms of quinone ring. In system 1 (Fig. 12C), negative character includes O20 and O21 atoms of the quinone ring. These negative centres of both systems **2** and 1 spontaneously constrained the electrophilic centre of target proteins. The surface hydrogen atoms of the alkyl chain had a neutral character. Also, the 1,2,3-bistriazole moieties had higher stability toward both acidic and basic hydrolysis. The 1,2,3-bistriazole moieties gave inertness for a variety of oxidizing and reducing chemicals.

2.3.4. Molecular docking analysis

*2.3.4.1. PPARγ – **2a** and GLUT4 – **2a**.* In the molecular docking analysis, the derivative **2a** showed promising interactions with PPARγ active sites of the ligand-binding domain. Interestingly, the second carbonyl of the ortho quinone moiety of embelin showed binding with ARG‘288; the first carbonyl of the ortho quinone moiety of embelin showed binding with SER‘342 and GLU‘343 (Fig. 13A). The binding energy (−7.72 kcal/mol), ligand efficiency (0.30) and inhibition constant (81.86 (mM)) also showed the efficacy of the compound **2a**. The full and partial agonist of PPARγ and their functions are based on the amino acid interactions with the drug molecules. For full agonists,

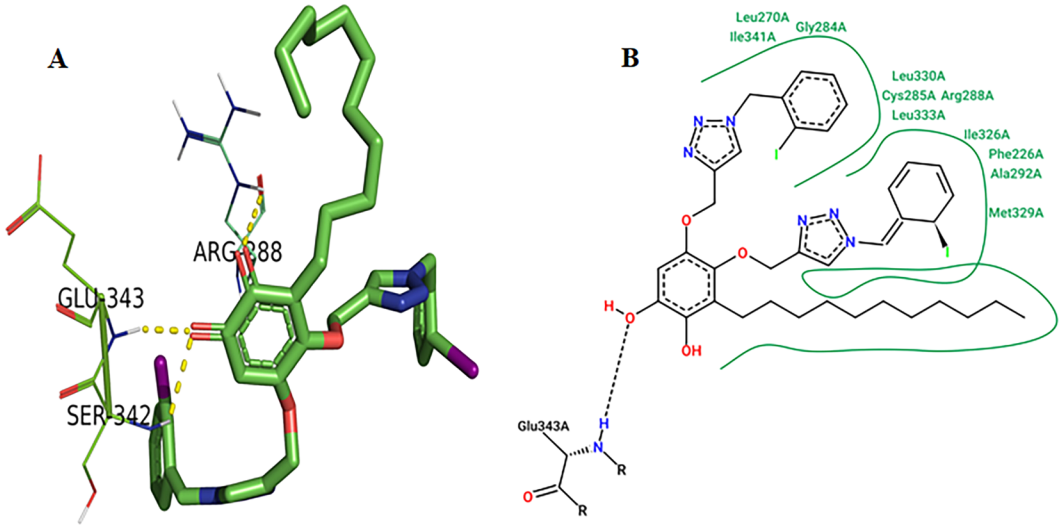

Fig. 13. Derivative **2a** with corresponding amino acid residues of PPARγ (A); hydrophobic interactions between Derivative **2a** and PPARγ (B); Yellow and Black dotted lines noted as hydrogen bonds.

the drug makes the hydrogen-bond interactions with SER 289, HIS 323, HIS 449, and TYR 473 residues, and partial agonists generally make the hydrogen bond with ARG 288 and SER 342 of PPARγ ligand-binding domain [89]. Cho et al. discussed that when the drug acts as a partial agonist of PPARγ, the conformational changes are different with different co-activators for mRNA transcription. This function makes the partial agonist of PPARγ, a selective PPARγ modulator and it may develop significant effects without any adverse effects [90]. This is in agreement with many previous publications [11,45,67,91–96]. Hence, the docking study insists and shows that the compound **2a** might act as a partial agonist of PPARγ.

When the compound activates PPARγ, it also regulates the expression of other genes such as GLUT4, which is more important to the regulation of glucose metabolism in the adipocyte [66,97,98]. In our study, the compound **2a** interacted with GLUT4 active sites in the transmembrane (TM) region. The first carbonyl of the ortho quinone moiety of embelin showed binding with GLN‘298 and the ortho quinone showed π-π interaction with PHE‘389. The triazole ring in the side chain at C-4 and C-5 showed π-π interaction with TYR‘309 and PHE‘460. The benzyl ring in the side chain at C-5 showed π-π interaction with PHE‘463 (Fig. 14A). Some TM regions especially TM7, are conserved with other glucose transporters like GLUT1 and the conserved residues are essential for glucose transportation. The TM7 region is a conserved motif at the exo-facial substrate-binding site of the glucose transporter channel, which acts as a selectivity filter for the passage of glucose [46,99].

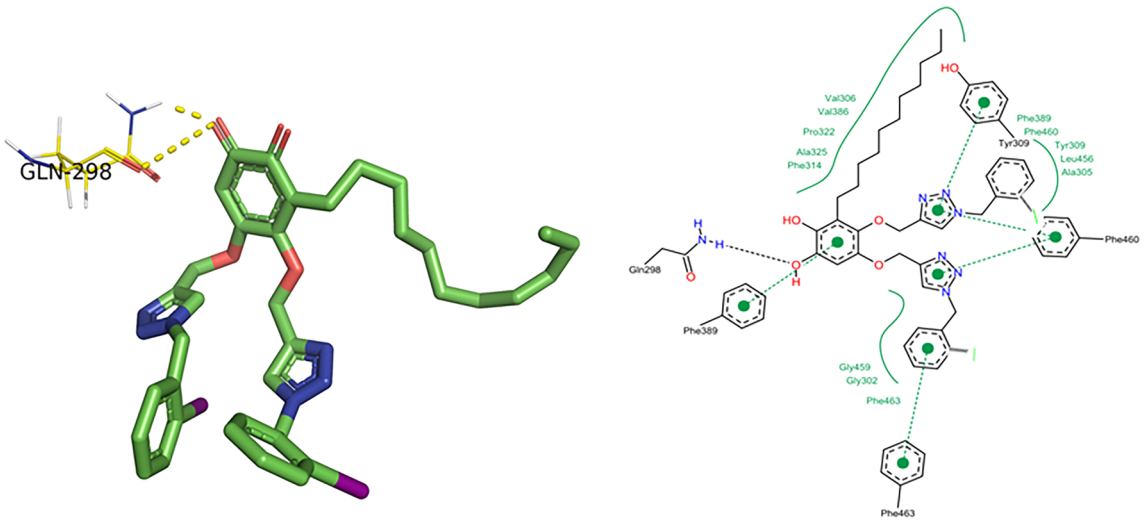

Fig. 14. Derivative **2a** with corresponding amino acid residues of GLUT4 (A); hydrophobic interactions between Derivative **2a** and GLUT4 (B); Yellow and Black dotted lines noted as hydrogen bonds.

Table 6
Molecular docking analysis.

Ligand	Protein(PDB ID)	Binding Residues	Binding Energy (kcal/mol)	Vdw_hb_ desolv_energy (kcal/mol)	Inhibition Constant	RMSD (Å)	Ligand efficiency
2a	PPAR Gamma(PDB ID: 2PRG)	ARG‘288/HE, GLU‘343/HN, SER‘342/HN	−7.72	−8.73	81.86 (mM)	60.77	0.30
2a	GLUT4 (Homology Model)	GLN‘298/O/1HE2	−6.82	−6.2	95.9 (mM)	43.47	0.28

Figs. 13B and 14B illustrate hydrophobic contacts of the docked derivative **2a** with active amino acids of 2PRG and GLUT4 (Modeled) and the interacting amino acid residues are given in the table (Table 6). The results obtained in this study indicated that the embelin based 1,2,3-bistriazole derivative (**2a**) up-regulated the PPARγ expression in adipose tissue with the translocation of GLUT4 activation in HFD-STZ induced diabetic rats.

3. Conclusion

In the present study, novel embelin-based 1,2,3-bistriazole moieties showed significant anti-diabetic effects in the HFD-STZ type 2 diabetic rats. The derivative **2a** (30 mg/kg) showed a significant effect in PPARγ and GLUT4 expression in epididymal adipose tissue. The measured biochemical parameters, electrostatic potential analysis and molecular docking studies extensively supported the activity of the molecule. Hence, this 1,2,3-bistriazole derivative enhanced the activity of embelin and could be a better drug for obesity-related T2DM.

4. Materials and methods

4.1. Plant material

The dried *Embelia ribes* Burm. (*Myrsinaceae*) fruits were acquired from the herbal farmhouse at Koyambedu, Chennai, India. It was authenticated by the plant taxonomist (Dr. M. Ayyanar) from the Department of Botany, Pachaiyappa's College, Chennai, India. The fruits were well-preserved (specimen no: ER/ERI/589) for future identification at the herbarium of the Entomology Research Institute, Loyola College, Chennai, India.

4.2. Chemicals and reagents

Streptozotocin (STZ) (Sigma-Aldrich, St. Louis, MO, USA), Taq polymerase, dNTPs, MMLV and primers - RT-PCR (GIBCO BRL, Rockville, MD), β-actin, PPARγ, GLUT4 and anti-insulin antibodies from Calbiochem (Darmstadt, Germany), ELISA kit and RNAiso Plus from Crystal Chem, Inc - Downers Grove, IL and Takara (Kusatsu, Japan), other Organic solvents from Merck (Darmstadt, Germany). All other chemicals and reagents used in this study were of analytical grade.

4.3. Isolation of embelin and synthesis of embelin –based 1,2,3-bistriazole (2a)

Embelin was isolated from *Embelia ribes* Burm. as described in the previously published article by Gandhi et al. [11,39]. The embelin-based 1,2,3-bistriazole was synthesized by propargylation of embelin followed by click reaction. Initially, potassium carbonate (1.04 g, 7.5 mmol) was added to the embelin (1) solution (1.47 g, 5 mmol) in DMF (20 mL) on stirring continuously at room temperature. To this solution, propargylbromide (0.7 mL, 7.5 mmol) was slowly added dropwise with stirring and the mixture continuously stirred overnight. Further extraction of the aqueous layer was done using DCM and repeated thrice. The combined organic extracts were dried over anhydrous Na_2SO_4, concentrated under vacuum to obtain the desired propargylated embelin (2′). By means of click chemistry, the obtained 2′ was converted to the bis-1,2,3-triazole derivative (**2a**). The latter was prepared by dissolving 2′ (1.1 g, 3 mmol) in 1:1 THF/H_2O mixture. To this solution, sodium azide (4 mmol), cuprous iodide (CuI) (catalytic amount) benzyl bromide (0.68 mL, 4 mmol) and triethylamine (0.7 mL, 5 mmol) were added. The ensuing solution was incubated in overnight stirring at room temperature. The reaction mixture was filtered, extracted with ethyl acetate and concentrated under vacuum. The crude **2a** was obtained and purified by using Column chromatography. The compound 2a was confirmed by spectral analysis such as NMR (Bruker NMR), and ESI-MS (Thermo Finnigan LCQ Advantage MAX 6000 ESI spectrometer) spectroscopic techniques (See Supplementary information).

4.4. Preparation of embelin –based 1,2,3-bistriazole (2a) suspension

For *in vivo* studies, the derivative **2a** was suspended in 0.5% sodium carboxymethylcellulose (CMC-Na) in warm water (1 mL/100 g) and used for the treatment in rats. The vehicle was used (CMC-Na (0.5%) thawed in warm water) individually at the dose of 1 mL/100 g for normal rats.

4.5. Animals

Around 5 weeks old adult male Albino Wistar rats (180 ± 10 g) were kept in the animal husbandry. The animal house was air-conditioned at 22 ± 1 °C, with the humidity range of 60 ± 5%. The rats were fed with standard pellet diet under the maintenance of 12/12 h day and night cycle for a week [11,39]. The used animals and experimental procedures were approved by the Institutional Animal Ethics Committee (Approval No: IAEC- ERI-LC-04/16).

4.6. Animal experiments

4.6.1. Acute oral toxicity study

Acute oral toxicity test was performed according to OECD (Organization for Economic Co-operation and Development) guideline test, ANNEX-423. These studies revealed that the derivative **2a** was safe at a maximum oral dose of 300 mg/kg b.w. in animals. No lethality or toxic reactions were observed in 14 days period. Based on this data, the optimal dose was fixed at 15 mg/kg (lower dose) and 30 mg/kg (higher dose) for further study.

4.6.2. Induction of diabetes

After acclimatization for a week, experimental rats were fed with a standard HFD as per the protocol of Gandhi et al. (Table 7) [45]. The normal control rats and the normal treated rats were fed with standard pellet diet. To induce T2DM, STZ (40 mg/kg) dissolved in citrate buffer (0.1 M with pH 4.5) was injected (1 mL/kg b wt.) into the rats by intraperitoneal injection. Citrate buffer was injected alone as a control to the normal rats [6]. The blood samples were taken from the tail vein of the rats after 5 days of the STZ injection and fasting blood glucose (FBG) > 250 mg/dl was considered as diabetic and added into the study [100].

4.6.3. Experimental grouping and treatment

The treatment setup and the animal group experiments were established as follows: 42 animals were randomly allocated into seven groups. Group I - Normal rats - vehicle (CMC-Na (0.5%) thawed in

Table 7
Composition of high-fat diet (%,W/W).

Ingredients	High-fat diet (g/kg)
Lard	310
Dalda (saturated fat)	110
Casein	250
Cholesterol	10
Cornstarch	120
Sucrose	85
Cellulose	50
Vitamin mixture	30
Mineral mixture	30
DL-Methionine	3
L-Cystine	1
Sodium chloride	1
Total metabolizable energy (kcal/kg)	5941

warm water) individually at the dose of 1 mL/100 g, Group II - Normal rats - derivative **2a** (15 mg/kg), Group III - Normal rats - derivative **2a** (30 mg/kg), Group IV - Diabetic rats – vehicle, Group V - Diabetic rats - derivative **2a** (15 mg/kg), Group VI - Diabetic rats - derivative **2a** (30 mg/kg) and Group VII - Diabetic rats - pioglitazone (10 mg/kg). All the treatments were orally administered by an intra-gastric tube once in a day for 28 days. Body weight of the animals was measured on day 0, day 14, day 21 and day 28 and the percent changes in body weight at each interval were calculated [17].

4.6.3.1. Bio-chemical estimation. In the biochemical analysis, the examination of FBG was analyzed every seventh day for 28 days. The Ultra-Sensitive Rat Insulin ELISA Kit (Crystal Chem, Inc. (USA)) was used to measure the plasma insulin level in the intervals of 0 and 28 days. In the meantime, the 15th day was chosen for the administration of OGTT. Afterward, the rats fasted 6 h with free water access; glucose solution (2 g/kg) was given to the rats by intra-gastric tube; before 30 min, the testing derivative molecule 2a and vehicle were administered to the rats. Blood glucose levels of all rats were tested initially before the glucose administration and 30, 60 and 120 min of post-glucose administration. In the study period, the diabetic rats fasted for six hours on the 25th day and the collected blood samples were gathered for the ITT. After the injection of treated rats with insulin (1.2 U/kg) via intra-peritoneal, the glucose level was administered between the time duration of 30 and 60 min.

The TG, TC, and FFA levels were assessed on 0 and 28th days [101–103]. At the end of the study period (30th day), all the treated rats were euthanized by gentle CO_2 anesthesia according to animal ethical regulations and serum was detached from the gathered blood samples by centrifugation.

The liver, skeletal muscles, pancreas, and adipose tissue were removed immediately from the rats and stored for further analysis. The homogenized liver was examined for hepatic enzymes such as hexokinase, glucose-6- phosphatase and fructose-1,6- bisphosphatase [104–107].

4.6.3.2. RT-PCT and western blotting analysis. To analyze the gene and protein expression, total RNA and protein of liver, skeletal muscle and adipose tissue (100 mg) were extracted from normal, diabetic control and derivative 2a treated diabetic rats. Followed by the detailed procedure of Stalin et al., the expression of two candidate genes and proteins PPARγ and GLUT4 were explored [11,39,70,108].

4.6.3.3. Histopathology. The histological sections (5 μm thickness) of the liver, adipose and pancreatic tissue of experimental rats were examined by the rotary microtome and spotted with H & E (Haematoxylin and Eosin) [109,110]. The samples were observed by the microscope (Leitz diaplan (40x) (Leica, Germany)).

4.7. Statistical analysis

All the statistical results were calculated by way of mean ± SEM. One-way ANOVA, followed by Dunnett's C posthoc test, was used to analyze the statistical difference among the groups. A two-tailed P value ≤ 0.01 was considered statistically significant.

4.8. Theoretical analysis

4.8.1. Ligand-protein selection

The structures of embelin based 1,2,3-bistriazole derivative **2a** and the standard control drug Pioglitazone was drawn by ChemDraw Ultra 12.0 and their bond errors were checked. To analyze the physicochemical properties of the derivative compound **2a**, the parent molecule embelin (1) and the derivative 6-Bromoembelin (2) have been chosen from our previous study [39]. The molecular and electronic structure calculations for embelin (1) and the derivative 6-Bromoembelin (2) were executed with density functional theory (DFT)/B3LYP method with 6-31G++ basis set for elements such C, H, N, O and basis set LanL2DZ for element I using the Gaussian09 program package [111] and the orbital analysis was completed with Gaussview v6.

Energy minimization and structural conformation of the ligand **2a** were done by the PRODRG server [112]. The 3D structure of the selected target protein PPARγ (PDB: 2PRG) was taken from the PDB database. The homology model of GLUT4 was done by modeler 9v10 and the model has been confirmed by Ramachandran Plot. The identification of active amino acid sites for the entire target proteins has as described earlier [11,39].

4.8.2. Docking analysis

The molecular docking analysis was executed by Auto dock tools [113]. The target protein molecules PPARγ and GLUT4 were presumed as a rigid body and the derivative molecule **2a** and Pioglitazone were being flexible. The affinity and electrostatic maps of all atoms of the ligands were assigned with a grid size of 126 × 126 × 126 in the spacing of 0.375 Å [114]. The Lamarckian Genetic Algorithm was used to identify the least energy binding of ligands. The docking was run for 10 generations with the default populations and mutation rate. The ligand-protein interaction was confirmed by the least binding energy conformation and the images of the interaction with the amino acids were generated by PyMol; two-dimensional hydrophobic interactions were developed by Pose View [115].

Declaration of Competing Interest

The authors declare that they have no known competing financial interests or personal relationships that could have appeared to influence the work reported in this paper.

Acknowledgments

The authors gratefully acknowledge the financial support provided by the Science and Engineering Research Board (SERB), Department of Science and Technology (DST), Government of India in the form of an award of National Post-Doctoral Fellowship (File No: PDF/2016/001235) and the Postdoctoral fund of Zhejiang Province (zj2019142), China to Dr. Antony Stalin. Also, this work was supported by the Key Research and Development Plan Project of Zhejiang Province (2017C02012).

Appendix A. Supplementary material

Supplementary data to this article can be found online at https://doi.org/10.1016/j.bioorg.2020.103579. These data include MOL files and InChiKeys of the most important compounds described in this article.

References

[1] L. Gelman, J.N. Feige, B. Desvergne, Molecular basis of selective PPARgamma modulation for the treatment of Type 2 diabetes, Biochim. Biophys. Acta 1771 (2007) 1094–1107.
[2] R.M. Evans, D.J. Mangelsdorf, Nuclear receptors, RXR, and the Big Bang, Cell 157 (2014) 255–266.
[3] K. Rikimaru, T. Wakabayashi, H. Abe, H. Imoto, T. Maekawa, O. Ujikawa, K. Murase, T. Matsuo, M. Matsumoto, C. Nomura, H. Tsuge, N. Arimura, K. Kawakami, J. Sakamoto, M. Funami, C.D. Mol, G.P. Snell, K.A. Bragstad, B.C. Sang, D.R. Dougan, T. Tanaka, N. Katayama, Y. Horiguchi, Y. Momose, A new class of non-thiazolidinedione, non-carboxylic-acid-based highly selective peroxisome proliferator-activated receptor (PPAR) gamma agonists: design and synthesis of benzylpyrazole acylsulfonamides, Bioorg. Med. Chem. 20 (2012) 714–733.
[4] F. Koohdani, G. Sotoudeh, Z. Kalantar, A. Mansoori, PPARgamma Pro12Ala polymorphism influences the relationship between dietary fat intake, adiposity and lipid profile in patients with Type 2 diabetes, Int. J. Vitam. Nutr. Res. 88

(2018) 263–269.
[5] T.M. Willson, M.H. Lambert, S.A. Kliewer, Peroxisome proliferator-activated receptor gamma and metabolic disease, Annu. Rev. Biochem. 70 (2001) 341–367.
[6] A.K. Sharma, S. Bharti, S. Goyal, S. Arora, S. Nepal, K. Kishore, S. Joshi, S. Kumari, D.S. Arya, Upregulation of PPARgamma by Aegle marmelos ameliorates insulin resistance and beta-cell dysfunction in high fat diet fed-streptozotocin induced type 2 diabetic rats, Phytother. Res. 25 (2011) 1457–1465.
[7] W.W. Cheatham, Peroxisome proliferator-activated receptor translational research and clinical experience, Am. J. Clin. Nutr. 91 (2010) 262S–266S.
[8] J.M. Olefsky, Treatment of insulin resistance with peroxisome proliferator-activated receptor gamma agonists, J. Clin. Invest. 106 (2000) 467–472.
[9] M. Ahmadian, J.M. Suh, N. Hah, C. Liddle, A.R. Atkins, M. Downes, R.M. Evans, PPARgamma signaling and metabolism: the good, the bad and the future, Nat. Med. 19 (2013) 557–566.
[10] L. Goedeke, R.J. Perry, G.I. Shulman, Emerging pharmacological targets for the treatment of nonalcoholic fatty liver disease, insulin resistance, and type 2 diabetes, Annu. Rev. Pharmacol. Toxicol. 59 (2019) 65–87.
[11] G.R. Gandhi, A. Stalin, K. Balakrishna, S. Ignacimuthu, M.G. Paulraj, R. Vishal, Insulin sensitization via partial agonism of PPARgamma and glucose uptake through translocation and activation of GLUT4 in PI3K/p-Akt signaling pathway by embelin in type 2 diabetic rats, Biochim. Biophys. Acta. 2013 (1830) 2243–2255.
[12] R. Joshi, J.P. Kamat, T. Mukherjee, Free radical scavenging reactions and antioxidant activity of embelin: biochemical and pulse radiolytic studies, Chem. Biol. Interact. 167 (2007) 125–134.
[13] S. Mahendran, S. Badami, V. Maithili, Evaluation of antidiabetic effect of embelin from Embelia ribes in alloxan induced diabetes in rats, Biomed. Preve. Nutr. 1 (2011) 25–31.
[14] N. Radhakrishnan, A. Gnanamani, A. Mandal, A potential antibacterial agent Embelin, a natural benzoquinone extracted from Embelia ribes, Biol. Med. 3 (2) (2011) 1–7.
[15] S. Durg, V.P. Veerapur, S. Neelima, S.B. Dhadde, Antidiabetic activity of Embelia ribes, embelin and its derivatives: a systematic review and meta-analysis, Biomed. Pharmacother. 86 (2017) 195–204.
[16] M.S. Alam, A. Ahad, L. Abidin, M. Aqil, S.R. Mir, M. Mujeeb, Embelin-loaded oral niosomes ameliorate streptozotocin-induced diabetes in Wistar rats, Biomed. Pharmacother. 97 (2018) 1514–1520.
[17] S.B. Dhadde, P. Nagakannan, M. Roopesh, S.R. Anand Kumar, B.S. Thippeswamy, V.P. Veerapur, S. Badami, Effect of embelin against 3-nitropropionic acid-induced Huntington's disease in rats, Biomed. Pharmacother. 77 (2016) 52–58.
[18] T. Yempala, J.P. Sridevi, P. Yogeeswari, D. Sriram, S. Kantevari, Rational design and synthesis of novel dibenzo[b, d]furan-1,2,3-triazole conjugates as potent inhibitors of Mycobacterium tuberculosis, Eur. J. Med. Chem. 71 (2014) 160–167.
[19] M. Yan, S. Ma, Recent advances in the research of heterocyclic compounds as antitubercular agents, Chem. Med. Chem. 7 (2012) 2063–2075.
[20] S. Gafner, J.L. Wolfender, M. Nianga, H. Stoeckli-Evans, K. Hostettmann, Antifungal and antibacterial naphthoquinones from Newbouldia laevis roots, Phytochemistry 42 (1996) 1315–1320.
[21] D.O. Moon, Y.H. Choi, N.D. Kim, Y.M. Park, G.Y. Kim, Anti-inflammatory effects of beta-lapachone in lipopolysaccharide-stimulated BV2 microglia, Int. Immunopharmacol. 7 (2007) 506–514.
[22] D.R. Buckle, B.C. Cantello, H. Smith, R.J. Smith, B.A. Spicer, Synthesis and antiallergic activity of 2-hydroxy-3-nitro-1,4-naphthoquinones, J. Med. Chem. 20 (1977) 1059–1064.
[23] T.P. Barbosa, C.A. Camara, T.M. Silva, R.M. Martins, A.C. Pinto, M.D. Vargas, New 1,2,3,4-tetrahydro-1-aza-anthraquinones and 2-aminoalkyl compounds from norlapachol with molluscicidal activity, Bioorg. Med. Chem. 13 (2005) 6464–6469.
[24] E. Perez-Sacau, A. Estevez-Braun, A.G. Ravelo, D. Gutierrez Yapu, A. Gimenez Turba, Antiplasmodial activity of naphthoquinones related to lapachol and beta-lapachone, Chem. Biodivers. 2 (2005) 264–274.
[25] M.J. Teixeira, Y.M. de Almeida, J.R. Viana, J.G. Holanda Filha, T.P. Rodrigues, J.R. Prata Jr., I.C. Coelho, V.S. Rao, M.M. Pompeu, In vitro and in vivo Leishmanicidal activity of 2-hydroxy-3-(3-methyl-2-butenyl)-1,4-naphthoquinone (lapachol), Phytother. Res. 15 (2001) 44–48.
[26] M. Ough, A. Lewis, E.A. Bey, J. Gao, J.M. Ritchie, W. Bornmann, D.A. Boothman, L.W. Oberley, J.J. Cullen, Efficacy of beta-lapachone in pancreatic cancer treatment: exploiting the novel, therapeutic target NQO1, Cancer. Biol. Ther. 4 (2005) 95–102.
[27] D.R. Buckle, H. Smith, B.A. Spicer, J.M. Tedder, Studies on v-triazoles. 9. Antiallergic 4,9-dihydro-4,9-dioxo-1H-naphtho[2,3-d]-v-triazoles, J. Med. Chem. 26 (1983) 714–719.
[28] S.G. Agalave, S.R. Maujan, V.S. Pore, Click chemistry: 1,2,3-triazoles as pharmacophores, Chem. Asian. J. 6 (2011) 2696–2718.
[29] B.S. Holla, M. Mahalinga, M.S. Karthikeyan, B. Poojary, P.M. Akberali, N.S. Kumari, Synthesis, characterization and antimicrobial activity of some substituted 1,2,3-triazoles, Eur. J. Med. Chem. 40 (2005) 1173–1178.
[30] D. Ashok, S. Gundu, V.K. Aamate, M.G. Devulapally, Microwave-assisted synthesis, antioxidant and antimicrobial evaluation of 2-indolinone-based bis-1,2,3-triazole derivatives, Mol. Divers. 22 (2018) 57–70.
[31] K.V. Schmidt, B.A. Wood, Trends in cancer therapy: role of monoclonal antibodies, Semin. Oncol. Nurs. 19 (2003) 169–179.
[32] M.C. Fernandes, E.N. Da Silva, A.V. Pinto, S.L. De Castro, R.F. Menna-Barreto, A novel triazolic naphthofuranquinone induces autophagy in reservosomes and impairment of mitosis in Trypanosoma cruzi, Parasitology 139 (2012) 26–36.
[33] S. Velazquez, R. Alvarez, C. Perez, F. Gago, E. De Clercq, J. Balzarini, M.J. Camarasa, Regiospecific synthesis and anti-human immunodeficiency virus activity of novel 5-substituted N-alkylcarbamoyl and N, N-dialkylcarbamoyl 1,2,3-triazole-TSAO analogues, Antivir. Chem. Chemother. 9 (1998) 481–489.
[34] R.A. Rane, P. Bangalore, S.D. Borhade, P.K. Khandare, Synthesis and evaluation of novel 4-nitropyrrole-based 1,3,4-oxadiazole derivatives as antimicrobial and antitubercular agents, Eur. J. Med. Chem. 70 (2013) 49–58.
[35] J.H. Cho, D.L. Bernard, R.W. Sidwell, E.R. Kern, C.K. Chu, Synthesis of cyclopentenyl carbocyclic nucleosides as potential antiviral agents against orthopoxviruses and SARS, J. Med. Chem. 49 (2006) 1140–1148.
[36] A. Kamal, P. Swapna, R.V. Shetti, A.B. Shaik, M.P. Narasimha Rao, F. Sultana, I.A. Khan, S. Sharma, N.P. Kalia, S. Kumar, B. Chandrakant, Anti-tubercular agents. Part 7: a new class of diarylpyrrole-oxazolidinone conjugates as antimycobacterial agents, Eur. J. Med. Chem. 64 (2013) 239–251.
[37] S.R. Naik, N.T. Niture, A.A. Ansari, P.D. Shah, Anti-diabetic activity of embelin: involvement of cellular inflammatory mediators, oxidative stress and other biomarkers, Phytomedicine 20 (2013) 797–804.
[38] R. Gupta, A.K. Sharma, M.C. Sharma, R.S. Gupta, Antioxidant activity and protection of pancreatic beta-cells by embelin in streptozotocin-induced diabetes, J. Diabetes 4 (2012) 248–256.
[39] A. Stalin, S.S. Irudayaraj, G.R. Gandhi, K. Balakrishna, S. Ignacimuthu, N.A. Al-Dhabi, Hypoglycemic activity of 6-bromoembelin and vilangin in high-fat diet fed-streptozotocin-induced type 2 diabetic rats and molecular docking studies, Life. Sci. 153 (2016) 100–117.
[40] K.K. Angajala, S. Vianala, R. Macha, M. Raghavender, M.K. Thupurani, P.J. Pathi, Synthesis, anti-inflammatory, bactericidal activities and docking studies of novel 1,2,3-triazoles derived from ibuprofen using click chemistry, Springerplus 5 (2016) 423.
[41] H.C. Kolb, M.G. Finn, K.B. Sharpless, Click chemistry: diverse chemical function from a few good reactions, Angew Chem. Int. Ed. Engl. 40 (2001) 2004–2021.
[42] P. Thirumurugan, D. Matosiuk, K. Jozwiak, Click chemistry for drug development and diverse chemical-biology applications, Chem. Rev. 113 (2013) 4905–4979.
[43] I. Abraham, R. Joshi, P. Pardasani, R.T. Pardasani, Recent advances in 1,4-benzoquinone chemistry, J. Braz. Chem. Soc. 22 (2011) 385–421.
[44] E. Krol, Z. Krejpcio, Evaluation of anti-diabetic potential of chromium(III) propionate complex in high-fat diet fed and STZ injected rats, Food. Chem. Toxicol. 49 (2011) 3217–3223.
[45] G.R. Gandhi, G. Jothi, P.J. Antony, K. Balakrishna, M.G. Paulraj, S. Ignacimuthu, A. Stalin, N.A. Al-Dhabi, Gallic acid attenuates high-fat diet fed-streptozotocin-induced insulin resistance via partial agonism of PPARgamma in experimental type 2 diabetic rats and enhances glucose uptake through translocation and activation of GLUT4 in PI3K/p-Akt signaling pathway, Eur. J. Pharmacol. 745 (2014) 201–216.
[46] V. Veerapur, K. Prabhakar, B. Thippeswamy, P. Bansal, K. Srinivasan, M. Unnikrishnan, Antidiabetic effect of Ficus racemosa Linn. stem bark in high-fat diet and low-dose streptozotocin-induced type 2 diabetic rats: a mechanistic study, Food. Chem. 132 (2012) 186–193.
[47] L. Zhang, J. Yang, X.Q. Chen, K. Zan, X.D. Wen, H. Chen, Q. Wang, M.X. Lai, Antidiabetic and antioxidant effects of extracts from Potentilla discolor Bunge on diabetic rats induced by high fat diet and streptozotocin, J. Ethnopharmacol. 132 (2010) 518–524.
[48] N. Vatandoust, F. Rami, A.R. Salehi, S. Khosravi, G. Dashti, G. Eslami, S. Momenzadeh, R. Salehi, Novel high-fat diet formulation and streptozotocin treatment for induction of prediabetes and type 2 diabetes in rats, Adv. Biomed. Res. 7 (2018) 107.
[49] X.Y. Li, S.S. Lu, H.L. Wang, G. Li, Y.F. He, X.Y. Liu, R. Rong, J. Li, X.C. Lu, Effects of the fenugreek extracts on high-fat diet-fed and streptozotocin-induced type 2 diabetic mice, Animal. Model. Exp. Med. 1 (2018) 68–73.
[50] J.Y. Kim, A. Nasr, H. Tfayli, F. Bacha, S.F. Michaliszyn, S. Arslanian, Increased lipolysis, diminished adipose tissue insulin sensitivity, and impaired beta-cell function relative to adipose tissue insulin sensitivity in obese youth with impaired glucose tolerance, Diabetes 66 (2017) 3085–3090.
[51] S.M. Jang, S.T. Yee, J. Choi, M.S. Choi, G.M. Do, S.M. Jeon, J. Yeo, M.J. Kim, K.I. Seo, M.K. Lee, Ursolic acid enhances the cellular immune system and pancreatic beta-cell function in streptozotocin-induced diabetic mice fed a high-fat diet, Int. Immunopharmacol. 9 (2009) 113–119.
[52] C.L. de Melo, M.G. Queiroz, S.G. Fonseca, A.M. Bizerra, T.L. Lemos, T.S. Melo, F.A. Santos, V.S. Rao, Oleanolic acid, a natural triterpenoid improves blood glucose tolerance in normal mice and ameliorates visceral obesity in mice fed a high-fat diet, Chem. Biol. Interact. 185 (2010) 59–65.
[53] M.F. Azevedo, C. Camsari, C.M. Sa, C.F. Lima, M. Fernandes-Ferreira, C. Pereira-Wilson, Ursolic acid and luteolin-7-glucoside improve lipid profiles and increase liver glycogen content through glycogen synthase kinase-3, Phytother. Res. 24 (Suppl 2) (2010) S220–S224.
[54] J. Liu, L. Han, L. Zhu, Y. Yu, Free fatty acids, not triglycerides, are associated with non-alcoholic liver injury progression in high fat diet induced obese rats, Lipids. Health. Dis. 15 (2016) 27.
[55] Y. Xin, Y. Wang, J. Chi, X. Zhu, H. Zhao, S. Zhao, Y. Wang, Elevated free fatty acid level is associated with insulin-resistant state in nondiabetic Chinese people, Diab. Metab. Syndr. Obes. 12 (2019) 139–147.
[56] K.F. Azman, Z. Amom, A. Azlan, N.M. Esa, R.M. Ali, Z.M. Shah, K.K. Kadir, Antiobesity effect of Tamarindus indica L. pulp aqueous extract in high-fat diet-induced obese rats, J. Nat. Med. 66 (2012) 333–342.
[57] R.B. Kasetti, M.D. Rajasekhar, V.K. Kondeti, S.S. Fatima, E.G. Kumar, S. Swapna, B. Ramesh, C.A. Rao, Antihyperglycemic and antihyperlipidemic activities of methanol:water (4:1) fraction isolated from aqueous extract of Syzygium alternifolium seeds in streptozotocin induced diabetic rats, Food. Chem. Toxicol. 48 (2010) 1078–1084.

[58] B.A. Aldahmash, D.M. El-Nagar, K.E. Ibrahim, Attenuation of hepatotoxicity and oxidative stress in diabetes STZ-induced type 1 by biotin in Swiss albino mice, Saudi. J. Biol. Sci. 23 (2016) 311–317.
[59] V. Rodriguez, L. Plavnik, N. Tolosa de Talamoni, Naringin attenuates liver damage in streptozotocin-induced diabetic rats, Biomed. Pharmacother. 105 (2018) 95–102.
[60] V.T. Samuel, G.I. Shulman, The pathogenesis of insulin resistance: integrating signaling pathways and substrate flux, J. Clin. Invest. 126 (2016) 12–22.
[61] R.K. Semple, V.K. Chatterjee, S. O'Rahilly, PPAR gamma and human metabolic disease, J. Clin. Invest. 116 (2006) 581–589.
[62] V. Dubois, J. Eeckhoute, P. Lefebvre, B. Staels, Distinct but complementary contributions of PPAR isotypes to energy homeostasis, J. Clin. Invest. 127 (2017) 1202–1214.
[63] B. Gross, M. Pawlak, P. Lefebvre, B. Staels, PPARs in obesity-induced T2DM, dyslipidaemia and NAFLD, Nat. Rev. Endocrinol. 13 (2017) 36–49.
[64] L. Zhang, K. Tian, Y. Li, L. Lei, A. Qin, L. Zhang, H. Song, L. Huo, L. Zhang, X. Jin, Z. Shen, Z. Feng, Novel phenyl-urea derivatives as dual-target ligands that can activate both GK and PPARγ, Acta Pharm. Sin. B 2 (2012) 588–597.
[65] M. Mueckler, Insulin resistance and the disruption of Glut4 trafficking in skeletal muscle, J. Clin. Invest. 107 (2001) 1211–1213.
[66] S.S. Irudayaraj, A. Stalin, C. Sunil, V. Duraipandiyan, N.A. Al-Dhabi, S. Ignacimuthu, Antioxidant, antilipidemic and antidiabetic effects of ficusin with their effects on GLUT4 translocation and PPARgamma expression in type 2 diabetic rats, Chem. Biol. Interact. 256 (2016) 85–93.
[67] J. Choi, Y. Park, H.S. Lee, Y. Yang, S. Yoon, 1,3-Diphenyl-1H-pyrazole derivatives as a new series of potent PPARgamma partial agonists, Bioorg. Med. Chem. 18 (2010) 8315–8323.
[68] E. Vargas, M.A. Carrillo Sepulveda, Physiology, Glucose Transporter Type 4 (GLUT4), in: StatPearls, Treasure Island (FL), 2019.
[69] S. Okuno, Y. Maeda, Y. Yamaguchi, Y. Takao, R.A. Trocino, H. Takino, E. Kawasaki, A. Yokota, S. Uotani, S. Akazawa, et al., Expression of GLUT4 glucose transporter mRNA and protein in skeletal muscle and adipose tissue from rats in late pregnancy, Biochem. Biophys. Res. Commun. 191 (1993) 405–412.
[70] Y.S. Lee, B.Y. Cha, K. Saito, H. Yamakawa, S.S. Choi, K. Yamaguchi, T. Yonezawa, T. Teruya, K. Nagai, J.T. Woo, Nobiletin improves hyperglycemia and insulin resistance in obese diabetic ob/ob mice, Biochem. Pharmacol. 79 (2010) 1674–1683.
[71] W.T. Garvey, L. Maianu, J.A. Hancock, A.M. Golichowski, A. Baron, Gene expression of GLUT4 in skeletal muscle from insulin-resistant patients with obesity, IGT, GDM, and NIDDM, Diabetes 41 (1992) 465–475.
[72] Y. Fukui, S. Masui, S. Osada, K. Umesono, K. Motojima, A new thiazolidinedione, NC-2100, which is a weak PPAR-gamma activator, exhibits potent antidiabetic effects and induces uncoupling protein 1 in white adipose tissue of KKAy obese mice, Diabetes 49 (2000) 759–767.
[73] M. Usui, S. Yamaguchi, Y. Tanji, R. Tominaga, Y. Ishigaki, M. Fukumoto, H. Katagiri, K. Mori, Y. Oka, H. Ishihara, Atf6alpha-null mice are glucose intolerant due to pancreatic beta-cell failure on a high-fat diet but partially resistant to diet-induced insulin resistance, Metabolism 61 (2012) 1118–1128.
[74] W. Xu, J. Morford, F. Mauvais-Jarvis, Emerging role of testosterone in pancreatic beta-cell function and insulin secretion, J. Endocrinol. 240 (2019) R97–R105.
[75] T. Kitamura, The role of FOXO1 in beta-cell failure and type 2 diabetes mellitus, Nat. Rev. Endocrinol. 9 (2013) 615–623.
[76] H. Yang, X. Li, The role of fatty acid metabolism and lipotoxicity in pancreatic β-cell injury: identification of potential therapeutic targets, Acta Pharm. Sin. B 2 (2012) 396–402.
[77] H. Alkhalidy, W. Moore, Y. Zhang, R. McMillan, A. Wang, M. Ali, K.S. Suh, W. Zhen, Z. Cheng, Z. Jia, M. Hulver, D. Liu, Small molecule kaempferol promotes insulin sensitivity and preserved pancreatic beta-cell mass in middle-aged obese diabetic Mice, J. Diab. Res. 2015 (2015) 532984.
[78] G.R. Gandhi, P. Vanlalhruaia, A. Stalin, S.S. Irudayaraj, S. Ignacimuthu, M.G. Paulraj, Polyphenols-rich Cyamopsis tetragonoloba (L.) Taub. beans show hypoglycemic and beta-cells protective effects in type 2 diabetic rats, Food Chem. Toxicol. 66 (2014) 358–365.
[79] A. Saxena, M. Bhatnagar, N.K. Garg, Enzymes changes in rat tissues during hyperglycemia, Arogya J. Health Sci. 10 (1984) 33–37.
[80] K. Fukui, Role of frontier orbitals in chemical reactions, Science. 218 (1982) 747–754.
[81] D.E. Manolopoulos, J.C. May, S.E. Down, Theoretical studies of the fullerenes: C34 to C70, Chem. Phys. Lett. 181 (1991) 105–111.
[82] J.-I. Aihara, Reduced HOMO−LUMO gap as an index of kinetic stability for polycyclic aromatic hydrocarbons, J. Phys. Chem. A 103 (1999) 7487–7495.
[83] Y. Ruiz-Morales, HOMO−LUMO gap as an index of molecular size and structure for Polycyclic Aromatic Hydrocarbons (PAHs) and asphaltenes: a theoretical study, Int. J. Phys. Chem. A 106 (2002) 11283–11308.
[84] T. Joselin Beaula, D. Manimaran, I. Hubert Joe, V.K. Rastogi, V. Bena Jothy, Vibrational spectroscopic studies and DFT computation of the nonlinear optical molecule L-Valinium formate, Spectrochim. Acta A Mol. Biomol. Spectrosc. 126 (2014) 170–177.
[85] E. Scrocco, J. Tomasi, P. Lowdin, Electronic molecular structure, reactivity and intermolecular forces: an euristic interpretation by means of electrostatic molecular potentials, Adv. Quant. Chem. 11 (1978) 115–193.
[86] R.G. Parr, L.V. Szentpaly, S. Liu, Electrophilicity Index, J. Am. Chem. Soc. 121 (1999) 1922–1924.
[87] A. Pirnau, V. Chis, M. Baias, O. Cozar, M. Vasilescu, O. Oniga, S. Simon, Experimental and DFT investigation of 5-para-nitro-benziliden-tiazolidin-2-tion-4-ona, J. Optoelectron. Adv. Mater. 9 (2007) 547–550.
[88] Y. Erdogdu, M. Guzel, M.T. Güllüoğlu, M. Amalanathan, S. Saglam, I.H. Joe, Molecular structure, vibrational spectral investigation and the confirmation analysis of 4-Methylesculetin molecule, Opt. Spectrosc. 116 (2014) 348–359.
[89] A. Stalin, S. Stephen Irudayaraj, D. Ramesh Kumar, K. Balakrishna, S. Ignacimuthu, N.A. Al-Dhabi, V. Duraipandiyan, Identifying potential PPARγ agonist/partial agonist from plant molecules to control type 2 diabetes using in silico and in vivo models, Med. Chem. Res. 25 (2016) 1980–1992.
[90] M.C. Cho, D.H. Lee, E.J. Kim, J.Y. Lee, J.W. Kang, J.H. Song, Y. Chong, Y. Kim, J.T. Hong, D.Y. Yoon, Novel PPARgamma partial agonists with weak activity and no cytotoxicity; identified by a simple PPARgamma ligand screening system, Mol. Cell. Biochem. 358 (2011) 75–83.
[91] I. Kouskoumvekaki, R.K. Petersen, F. Fratev, O. Taboureau, T.E. Nielsen, T.I. Oprea, S.B. Sonne, E.N. Flindt, S.O. Jonsdottir, K. Kristiansen, Discovery of a novel selective PPARgamma ligand with partial agonist binding properties by integrated in silico/in vitro work flow, J. Chem. Inf. Model. 53 (2013) 923–937.
[92] L. Guasch, E. Sala, C. Valls, M. Blay, M. Mulero, L. Arola, G. Pujadas, S. Garcia-Vallve, Structural insights for the design of new PPARgamma partial agonists with high binding affinity and low transactivation activity, J. Comput. Aided. Mol. Des. 25 (2011) 717–728.
[93] L. Guasch, E. Sala, A. Castell-Auvi, L. Cedo, K.R. Liedl, G. Wolber, M. Muehlbacher, M. Mulero, M. Pinent, A. Ardevol, C. Valls, G. Pujadas, S. Garcia-Vallve, Identification of PPARgamma partial agonists of natural origin (I): development of a virtual screening procedure and in vitro validation, PLoS One 7 (2012) e50816.
[94] C.S. Mizuno, A.G. Chittiboyina, F.H. Shah, A. Patny, T.W. Kurtz, H.A. Pershadsingh, R.C. Speth, V.T. Karamyan, P.B. Carvalho, M.A. Avery, Design, synthesis, and docking studies of novel benzimidazoles for the treatment of metabolic syndrome, J. Med. Chem. 53 (2010) 1076–1085.
[95] A.C. Puhl, A. Bernardes, R.L. Silveira, J. Yuan, J.L. Campos, D.M. Saidemberg, M.S. Palma, A. Cvoro, S.D. Ayers, P. Webb, P.S. Reinach, M.S. Skaf, I. Polikarpov, Mode of peroxisome proliferator-activated receptor gamma activation by luteolin, Mol. Pharmacol. 81 (2012) 788–799.
[96] K. Yamagishi, K. Yamamoto, Y. Mochizuki, T. Nakano, S. Yamada, H. Tokiwa, Flexible ligand recognition of peroxisome proliferator-activated receptor-gamma (PPARgamma), Bioorg. Med. Chem. Lett. 20 (2010) 3344–3347.
[97] O. Dubuisson, E.J. Dhurandhar, R. Krishnapuram, H. Kirk-Ballard, A.K. Gupta, V. Hegde, E. Floyd, J.M. Gimble, N.V. Dhurandhar, PPARgamma-independent increase in glucose uptake and adiponectin abundance in fat cells, Endocrinology 152 (2011) 3648–3660.
[98] Y. Zhang, H. Zhang, X.G. Yao, H. Shen, J. Chen, C. Li, L. Chen, M. Zheng, J. Ye, L. Hu, X. Shen, H. Jiang, (+)-Rutamarin as a dual inducer of both GLUT4 translocation and expression efficiently ameliorates glucose homeostasis in insulin-resistant mice, PLoS One. 7 (2012) e31811.
[99] S.S. Mohan, J.J. Perry, N. Poulose, B.G. Nair, G. Anilkumar, Homology modeling of GLUT4, an insulin regulated facilitated glucose transporter and docking studies with ATP and its inhibitors, J. Biomol. Struct. Dyn. 26 (2009) 455–464.
[100] P. Trinder, Determination of glucose in blood using glucose oxidase with an alternative oxygen acceptor, Ann. Clin. Biochem. 6 (1969) 24–27.
[101] A.A. Henley, The determination of serum cholesterol, Analyst 82 (1957) 286–287.
[102] L.B. Foster, R.T. Dunn, Stable reagents for determination of serum triglycerides by a colorimetric Hantzsch condensation method, Clin. Chem. 19 (1973) 338–340.
[103] K. Itaya, M. Ui, Colorimetric determination of free fatty acids in biological fluids, J. Lipid. Res. 6 (1965) 16–20.
[104] N. Brandstrup, J.E. Kirk, C. Bruni, Determination of hexokinase in tissues, J. Gerontol. 12 (1957) 166–171.
[105] J.M. Gancedo, C. Gancedo, Fructose-1,6-diphosphatase, phosphofructokinase and glucose-6-phosphate dehydrogenase from fermenting and non fermenting yeasts, Arch. Mikrobiol. 76 (1971) 132–138.
[106] H. Koide, T. Oda, Pathological occurrence of glucose-6-phosphatase in serum in liver diseases, Clin. Chim. Acta 4 (1959) 554–561.
[107] E. Van Handel, Estimation of glycogen in small amounts of tissue, Anal. Biochem. 11 (1965) 256–265.
[108] V.S. Muthusamy, C. Saravanababu, M. Ramanathan, R. Bharathi Raja, S. Sudhagar, S. Anand, B.S. Lakshmi, Inhibition of protein tyrosine phosphatase 1B and regulation of insulin signalling markers by caffeoyl derivatives of chicory (Cichorium intybus) salad leaves, Br. J. Nutr. 104 (2010) 813–823.
[109] G.R. Gandhi, S. Ignacimuthu, M.G. Paulraj, Hypoglycemic and beta-cells regenerative effects of Aegle marmelos (L.) Corr. bark extract in streptozotocin-induced diabetic rats, Food. Chem. Toxicol. 50 (2012) 1667–1674.
[110] N.P. Babu, P. Pandikumar, S. Ignacimuthu, Anti-inflammatory activity of Albizia lebbeck Benth., an ethnomedicinal plant, in acute and chronic animal models of inflammation, J. Ethnopharmacol. 125 (2009) 356–360.
[111] G.W.T.M.J. Frisch, H.B. Schlegel, G.E. Scuseria, M.A. Robb, J.R. Cheeseman, G. Scalmani, V. Barone, G.A. Petersson, H. Nakatsuji, X. Li, M. Caricato, et al., Gaussian 09, Revision A.02, Gaussian, Inc., Wallingford CT, 2016.
[112] A.W. Schuttelkopf, D.M. van Aalten, PRODRG: a tool for high-throughput crystallography of protein-ligand complexes, Acta. Crystallogr. D. Biol. Crystallogr. 60 (2004) 1355–1363.
[113] G.M. Morris, R. Huey, W. Lindstrom, M.F. Sanner, R.K. Belew, D.S. Goodsell, A.J. Olson, AutoDock4 and AutoDockTools4: automated docking with selective receptor flexibility, J. Comput. Chem. 30 (2009) 2785–2791.
[114] R. Huey, G.M. Morris, A.J. Olson, D.S. Goodsell, A semiempirical free energy force field with charge-based desolvation, J. Comput. Chem. 28 (2007) 1145–1152.
[115] K. Stierand, M. Rarey, Drawing the PDB: protein-ligand complexes in two dimensions, ACS Med. Chem. Lett. 1 (2010) 540–545.